Correlation of response spectral values in Japanese ground motions

Nirmal Jayaram[1], Jack W. Baker[*1], Hajime Okano[2], Hiroshi Ishida[2],
Martin W. McCann, Jr.[1] and Yoshinori Mihara[2]

[1]*Department of Civil and Environmental Engineering, Stanford University, 473 Via Ortega, Room 283,
Stanford, 94305, California, USA*
[2]*Kajima Corporation, 6-5-30 Akasaka, Minato-ku, Tokyo, 107-8502, Japan*

Abstract. Ground motion models predict the mean and standard deviation of the logarithm of spectral acceleration, as a function of predictor variables such as earthquake magnitude, distance and site condition. Such models have been developed for a variety of seismic environments throughout the world. Some calculations, such as the Conditional Mean Spectrum calculation, use this information but additionally require knowledge of correlation coefficients between logarithmic spectral acceleration values at multiple periods. Such correlation predictions have, to date, been developed primarily from data recorded in the Western United States from active shallow crustal earthquakes. This paper describes results from a study of spectral acceleration correlations from Japanese earthquake ground motion data that includes both crustal and subduction zone earthquakes. Comparisons are made between estimated correlations for Japanese response spectral ordinates and correlation estimates developed from Western United States ground motion data. The effect of ground motion model, earthquake source mechanism, seismic zone, site conditions, and source to site distance on estimated correlations is evaluated and discussed. Confidence intervals on these correlation estimates are introduced, to aid in identifying statistically significant differences in correlations among the factors considered. Observed general trends in correlation are similar to previous studies, with the exception of correlation of spectral accelerations between orthogonal components, which is seen to be higher here than previously observed. Some differences in correlations between earthquake source zones and earthquake mechanisms are observed, and so tables of correlations coefficients for each specific case are provided.

Keywords: ground motion; intensity measure; correlation; risk analysis.

1. Introduction

Ground motion models predict the mean and standard deviation of the logarithm of spectral acceleration, and are widely used in probabilistic seismic hazard analyses (PSHA). These models can be further extended by supplementing them with predictions of the correlation between response spectral values at differing periods or orientations. Several such models have been developed in the past (Abrahamson *et al*. 2003, Baker and Cornell 2006a, Baker and Jayaram 2008, Gulerce and Abrahamson 2011, Inoue and Cornell 1990), based either on U.S. data, or data from around the

---

* Corresponding author, Professor, E-mail: bakerjw@stanford.edu

world. The only such model to use primarily Japanese ground motions was by Ishida (1993), but that work was based on a much more limited ground motion data set than is available today.

This paper performs an evaluation of response spectrum correlations observed from a large database of Japanese strong ground motions. Evaluations are made to determine the possible impact of rupture mechanism, site conditions, crustal source zone and ground motion model on observed correlations. Observed correlations are also compared to the predictive model of Baker and Jayaram (2008), to determine the applicability of that model for use with Japanese ground motions and other earthquake sources (the Baker and Jayaram model was developed for active shallow crustal earthquakes). The results further our understanding of how these correlations vary from one geographic region to another, and will be useful for future applications of Vector-valued Probabilistic Seismic Hazard Analysis (Bazzurro and Cornell 2002, Bazzurro *et al.* 2009) and Conditional Mean Spectrum (Baker and Cornell 2006b) calculations at Japanese sites.

2. Ground motion data

The ground motion records were obtained from K-NET and KiK-net (Aoi *et al.* 2000, Kinoshita 1998), the digital strong-motion seismograph networks deployed by National Research Institute for Earth Science and Disaster Prevention (NIED) across Japan. Ground motions that met the following criteria were selected: the earthquake magnitude M_j was greater or equal to 6.4 and the closest fault distance X_{cl} was less than or equal to 200 km. All ground motions were recorded after June 1996, when the K-NET service began operation. All of these ground motions were recorded at the ground surface and in the free-field (i.e. the subsurface recordings available from KiK-net were not used). A total of 2819 ground motions were collected, and are reported Table 1 grouped by fault distance and NEHRP site classification (Building Seismic Safety Council 1997).

The M_j is earthquake magnitude determined by Japan Meteorological Agency (JMA), although moment magnitude M_w is also used in the following study. The lowest magnitude was chosen as 6.4. The dataset include several inland shallow crustal earthquakes whose magnitudes are approximately M_j = 7.0. The largest earthquake in the dataset is the 2003 M_j = 8.0 Tokachi-oki Earthquake. The closest fault distance X_{cl} was determined using the fault plane evaluated by the Geospatial Information Authority of Japan (GSI). When the fault plane was not provided by GSI, the hypocentral distance determined by JMA was used. The cutoff frequency of seismographs used in K-NET and KiK-net are 30 Hz (period of 0.033 seconds). Response spectral values are known to be affected by this cutoff, and so only periods greater than 0.05 seconds are considered in the analysis. The longest usable period of each ground motion was determined by examining the Fourier spectrum to determine when the signal to noise ratio is acceptable, and ground motions were only

Table 1 Number of selected ground motions, categorized by distance and site class

Fault Distance	NEHRP site classification[1]					Total
	A	B	C	D	E	
X_{cl} < 100 km	1	50	310	208	9	578
100 km < X_{cl} < 200 km	3	204	1157	839	38	2241

[1]A: $Vs30 \geq 1500$ m/s, B: 760 m/s$\leq Vs30 < 1500$ m/s, C: 360 m/s $\leq Vs30 < 760$ m/s,
D: 180 m/s $\leq Vs30 < 360$ m/s, E: $Vs30 < 180$ m/s

used for periods smaller than their longest usable period. The ground motion model used below to compute spectral accelerations (Kanno *et al*. 2006) requires V_{s30} (average shear-wave velocity to 30m depth) as a predictor variable, so V_{s30} values were collected for all sites. For the K-NET stations, where only V_{s20} values are available, inferred V_{s30} values were obtained for each V_{s20} value using the model provided by Kanno *et al*. (2006). Finally, the ground motion model requires knowledge of the distance between the Kuril, Japan, and Izu-Bonin trenches; this distance was computed for each recording using the provided latitude and longitude information for the recording stations.

3. Correlation calculations

To evaluate the correlation between spectral ordinates at different periods, first consider the form of standard ground motion models. Predictions of spectral accelerations take the following form

$$\ln Sa(T) = \mu_{\ln Sa}(M, R, \theta, T) + \sigma_{\ln Sa}(T)\varepsilon(T) \tag{1}$$

where $\mu_{\ln Sa}(M, R, \theta, T)$ is the predicted mean of the natural log of spectral acceleration (*Sa*) at a specified period (*T*), as predicted by the ground motion model. This predicted mean is a function of earthquake magnitude (*M*), source-to-site distance (*R*), and other parameters (θ) such as local site conditions and faulting mechanism. The term $\sigma_{\ln Sa}(T)$ is the predicted standard deviation of ln*Sa*, also provided by the ground motion model. The term $\varepsilon(T)$ represents the number of standard deviations by which the actual logarithmic spectral acceleration, ln*Sa*(*T*), differs from its predicted mean value $\mu_{\ln Sa}(M, R, \theta, T)$. For observed ground motions with known *Sa*(*T*) and known *M*, *R*, etc., $\varepsilon(T)$ is a known number. For future ground motions, $\varepsilon(T)$ is represented by a random variable with a mean value of zero and standard deviation of one. For the results presented here, the $\mu_{\ln Sa}(M, R, \theta, T)$ and $\sigma_{\ln Sa}(T)$ values are obtained from the ground motion model of Kanno *et al*. (2006), a modern model for Japanese ground motions. This model uses focal depth, average site shear wave velocity over the top 30 m, and shortest distance from the site to the Kuril and Izu-Bonin trenches as additional predictor parameters (denoted θ here).

Solving equation for $\varepsilon(T)$, we see that if a ground motion response spectrum has been observed, and its associated magnitude, distance, etc. are known, then $\varepsilon(T)$ can be computed as

$$\varepsilon(T) = \frac{\ln Sa(T) - \mu_{\ln Sa}(M, R, \theta, T)}{\sigma_{\ln Sa}(T)} \tag{2}$$

These ε values vary with period and thus are explicitly denoted as a function of period above. Fig. 1 graphically illustrates the terms on the right hand side of Eq. (2) (i.e. observed and predicted spectral values, along with +/- standard deviations around predicted spectral values), and shows computed ε values for three periods. This illustrates how $\varepsilon(T)$ varies for real response spectra that have "peaks" and "valleys" as they vary across periods.

Using Eq. (2), we can compute $\varepsilon(T)$ values for the entire ground motion library described in the previous section, and then estimate the correlation coefficients between these ε values at two periods $\varepsilon(T_1)$ and $\varepsilon(T_2)$. The Pearson product-moment correlation coefficient (Kutner *et al*. 2004), one common estimator of correlation coefficients from empirical data, is computed as follows
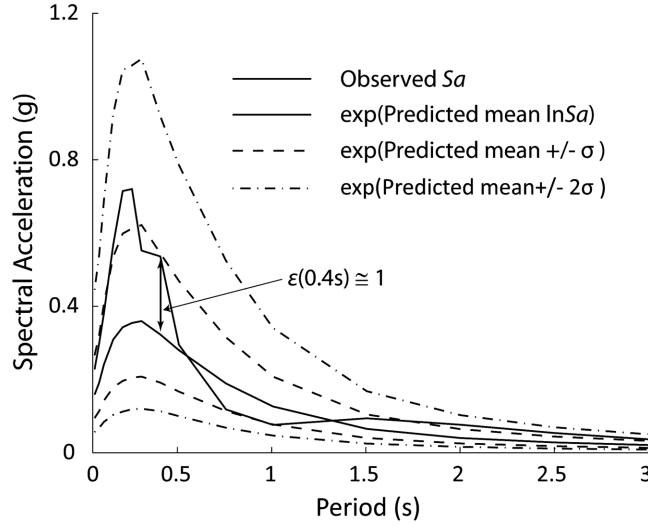
Fig. 1 Response spectrum of a ground motion from the 2000 M_j = 7.3 Western Honshu Earthquake, recorded at distance of 23km. Also shown are the predicted $\mu_{\ln Sa}(M,R,\theta,T)$, and $+/-\sigma_{\ln Sa}(T)$ bounds from the Kanno *et al.* (2006) ground-motion model, and an illustration of the $\varepsilon(T)$ term

$$\rho_{\varepsilon(T_1),\,\varepsilon(T_2)} = \frac{\sum\limits_{i=1}^{n}(\varepsilon_i(T_1) - \overline{\varepsilon(T_1)})(\varepsilon_i(T_2) - \overline{\varepsilon(T_2)})}{\sqrt{\sum\limits_{i=1}^{n}(\varepsilon_i(T_1) - \overline{\varepsilon(T_1)})^2 \sum\limits_{i=1}^{n}(\varepsilon_i(T_2) - \overline{\varepsilon(T_2)})^2}} \tag{3}$$

where $\varepsilon_i(T_1)$ and $\varepsilon_i(T_2)$ are the *i*th observations of $\varepsilon(T_1)$ and $\varepsilon(T_2)$, $\overline{\varepsilon(T_1)}$ and $\overline{\varepsilon(T_2)}$ are their sample means, and n is the number of considered ground motions.

One goal of this work is to determine whether existing predictive models for correlations perform well for these Japanese ground motions, so the empirical correlations obtained from Eq. (3) will be compared to the predictive model by Baker and Jayaram (2008). That predictive model is evaluated by first computing the following initial coefficients

$$C_1 = 1 - \cos\left(\frac{\pi}{2} - 0.366\ln\left(\frac{T_{\max}}{\max(T_{\min,\,0.109})}\right)\right)$$

$$C_2 = \begin{cases} 1 - 0.105\left(1 - \dfrac{1}{1 + e^{100T_{\max} - 5}}\right)\left(\dfrac{T_{\max} - T_{\min}}{T_{\max} - 0.0099}\right) & \text{if } T_{\max} < 0.2 \\ 0 & \text{otherwise} \end{cases} \tag{4}$$

$$C_3 = \begin{cases} C_2 & \text{if } T_{\max} < 0.109 \\ C_1 & \text{otherwise} \end{cases}$$

$$C_4 = C_1 + 0.5(\sqrt{C_3} - C_3)\left(1 + \cos\left(\frac{\pi T_{\min}}{0.109}\right)\right)$$

where $T_{min} = \min(T_1,T_2)$ and $T_{max} = \max(T_1,T_2)$. The predicted correlation coefficient is then given by

$$
\begin{array}{lll}
\text{if} \;\; T_{max} < 0.109 & \rho_{\varepsilon(T_1),\,\varepsilon(T_2)} = C_2 \\
\text{else if} \;\; T_{min} > 0.109 & \rho_{\varepsilon(T_1),\,\varepsilon(T_2)} = C_1 \\
\text{else if} \;\; T_{max} < 0.2 & \rho_{\varepsilon(T_1),\,\varepsilon(T_2)} = \min(C_2, C_4) \\
\text{else} & \rho_{\varepsilon(T_1),\,\varepsilon(T_2)} = C_4
\end{array}
\tag{5}
$$

This predictive model was obtained by following the procedure described in this section and computing correlations using Eq. (3), but using a dataset containing ground motions from active shallow crustal earthquakes around the world. The observed correlations were then approximately reproduced by the analytical functions in Eqs. (4) and (5).

4. Results

Using the procedure and ground motions described above, correlation coefficients were computed for a variety of cases, and the results are summarized and presented in this section. Fig. 2(a) shows correlation coefficients between spectral acceleration residuals (the numerical values from this figure are provided in Table 2 of the appendix). Each line in the plot represents a specific T_2 value, the x axis shows varying T_1 values, and the y axis shows $\rho_{\varepsilon(T_1),\,\varepsilon(T_2)}$ as computed using Eq. (3). The $\varepsilon(T)$ values used in Eq. (3) were computed using Eq. (2), with the Kanno *et al.* (2006) ground-motion model used to compute the predicted mean square root of the sum of squares and standard deviations for each observed response spectral value. Results are presented for periods between 0.05s and 4s, approximately spanning the range of periods considered by the Kanno *et al.* (2006) model.
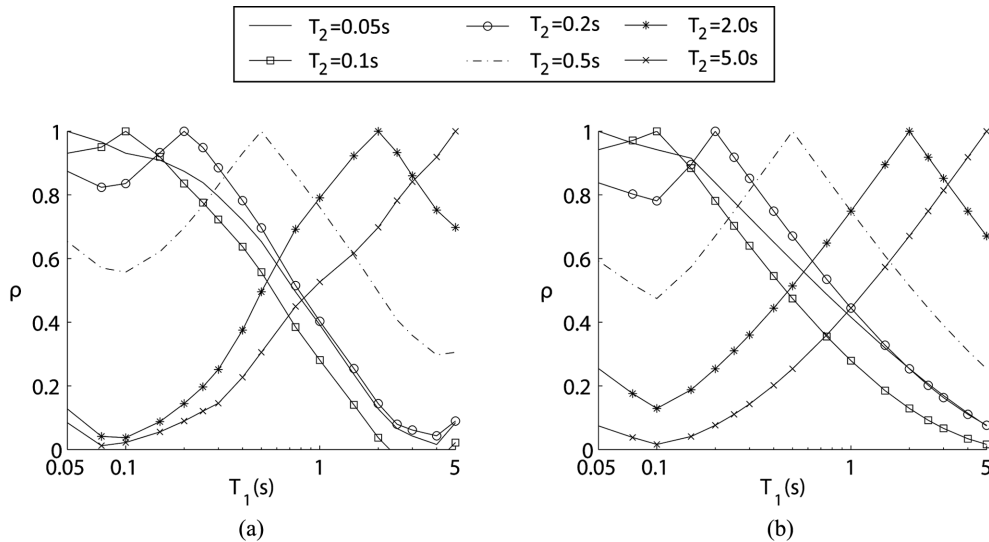

Fig. 2 Plots of correlation coefficients of $\varepsilon(T_1)$ versus $\varepsilon(T_2)$: (a) estimated using residuals from the Kanno *et al.* (2006) ground-motion model and (b) predicted by the Baker and Jayaram (2008) correlation model

Fig. 2(b) shows the corresponding correlation coefficients predicted by Eqs. (4) and (5). It can be seen from comparisons of Fig. 2(a) and 2(b) that the correlations obtained using the Japanese ground motions show trends that are similar to the correlations from the predictive model. Differences are observed between the correlations in the two cases when T_1 and T_2 differ significantly (in particular, when one period is shorter than 0.1s and the other longer than 2.0s).

It is also of interest to detect variations in correlations from subsets of the overall ground motion library, so a variety of additional evaluations were performed. In order to assess the impact of earthquake source zone on the correlation, the data set was subdivided into three groups, and the correlations computed separately for each group. Fig. 3 shows the correlation estimates obtained using ground motions from active crustal zone, subduction interface zone and subduction slab zone earthquakes respectively. The number of ground motions in each of these subsets is noted in the figure caption.

The subduction slab zone earthquakes have higher stress drops and relatively richer short-period energy than the subduction interface zone earthquakes. The active shallow crustal earthquakes may have differing relative energy at short and long periods as well, because they tend to be recorded at shorter distances where attenuation of short period energy has not been as significant. These differences affect the shape of resulting response spectra, which could cause differences in observed correlations between these groups of ground motions. Differences in mean spectra should in principle be accounted for by the $\mu_{\ln Sa}(M, R, \theta, T)$ term of Eq. (1), so that the correlation coefficients primarily quantify the peak-to-valley variability (i.e. "bumpiness") of the spectra about the mean. On the other hand, differences in correlation may result if the ground motion model's $\mu_{\ln Sa}(M, R, \theta, T)$ does not fully capture differences in mean spectral shape between these source zones. To quantitatively evaluate the differences in correlations observed in Fig. 3, one can use statistical hypothesis testing.

The estimates of correlations have statistical uncertainty due to the finite number of ground motions used to estimate these correlation values (Kutner *et al.* 2004). This uncertainty, which is a function of the number of observations used to obtain the estimate, can be explicitly evaluated. Further, the uncertainty in the correlation is smaller when the estimated correlation coefficient is close to -1 or +1. This uncertainty can be quantified and used to compare correlations estimated using two groups of observations G1 and G2 (e.g. ground motions from subduction interface zone earthquakes and active shallow crustal earthquakes). This is done by constructing an "acceptance region" around the correlation estimated using G1 and verifying whether the estimated correlation using G2 falls within the acceptance region. The acceptance region is constructed such that if the correlations from G2 fall within the acceptance region, the differences in the correlations estimated using the two groups are statistically insignificant at the 95% significance level (Kutner *et al.* 2004). If the correlations from G2 fall outside of the acceptance region, there is less than a 5% chance that we would have observed this difference due simply to the finite number of ground motions. Fig. 4 shows the estimated correlations from the subduction interface zone earthquake ground motions (the same correlations shown in Fig. 3(b)) for selected period pairs, along with the acceptance region for comparison to the correlations for active shallow crustal earthquake ground motions at the same period pairs. We see in many cases that the correlations from subduction interface zone and active shallow crustal earthquake ground motions differ by an amount larger than indicated by the acceptance region, suggesting that differences are not likely to be due to the finite sample size alone; there may be systematic differences between these analysis cases. As discussed above, this may be due to differences in the average frequency characteristics of ground motions from these
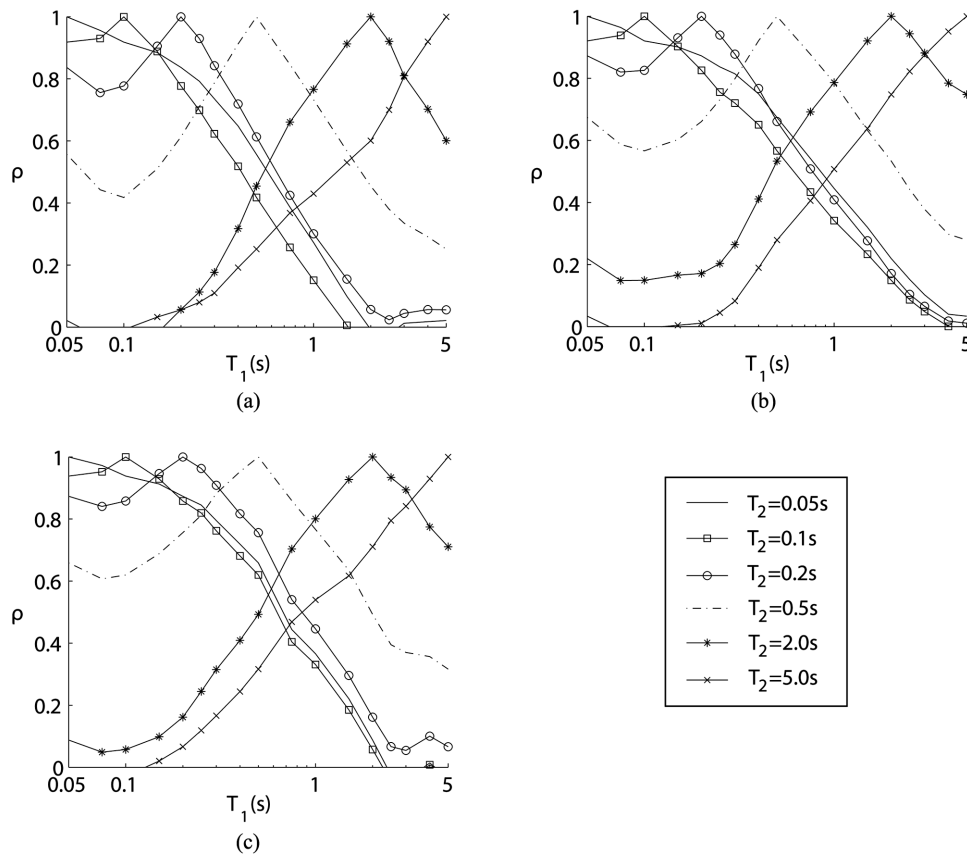
Fig. 3 Plots of correlation coefficients of $\varepsilon(T_1)$ versus $\varepsilon(T_2)$ estimated using ground motions corresponding to (a) active shallow crustal zone earthquakes (1281 records), (b) subduction interface zone earthquakes (936 records) and (c) subduction slab zone earthquakes (602 records)

two classes of earthquakes that are not accounted for by the ground motion model.

The standard acceptance region calculation carried out here assumes that observed data used to compute the correlations are independent. That assumption is not strictly valid in this case, as multiple ground motions come from single earthquakes, and ground motions recorded at spatially adjacent sites tend to have correlated response spectra. This dependence would broaden the resulting acceptance region. There is no analytical technique available to estimate these acceptance regions for correlations for non-independent observations, and it is expected that conclusions of the paper would not be changed by considering this effect, so further investigation was not performed.

Since some correlations appear to vary somewhat with earthquake source, as well as with other parameters discussed below, selected tables of correlation coefficients for various cases are provided in an appendix. Correlation coefficients for the three cases plotted in Fig. 3 are provided in Table 3 through Table 5.

To assess the impact of earthquake mechanism, the ground motions from normal faults, oblique faults, reverse faults and strike-slip faults were considered separately, and correlations computed for each group individually. Fig. 5 shows plots of these correlations, which are also provided numerically in Table 6 through Table 9. The figure shows some differences between the different
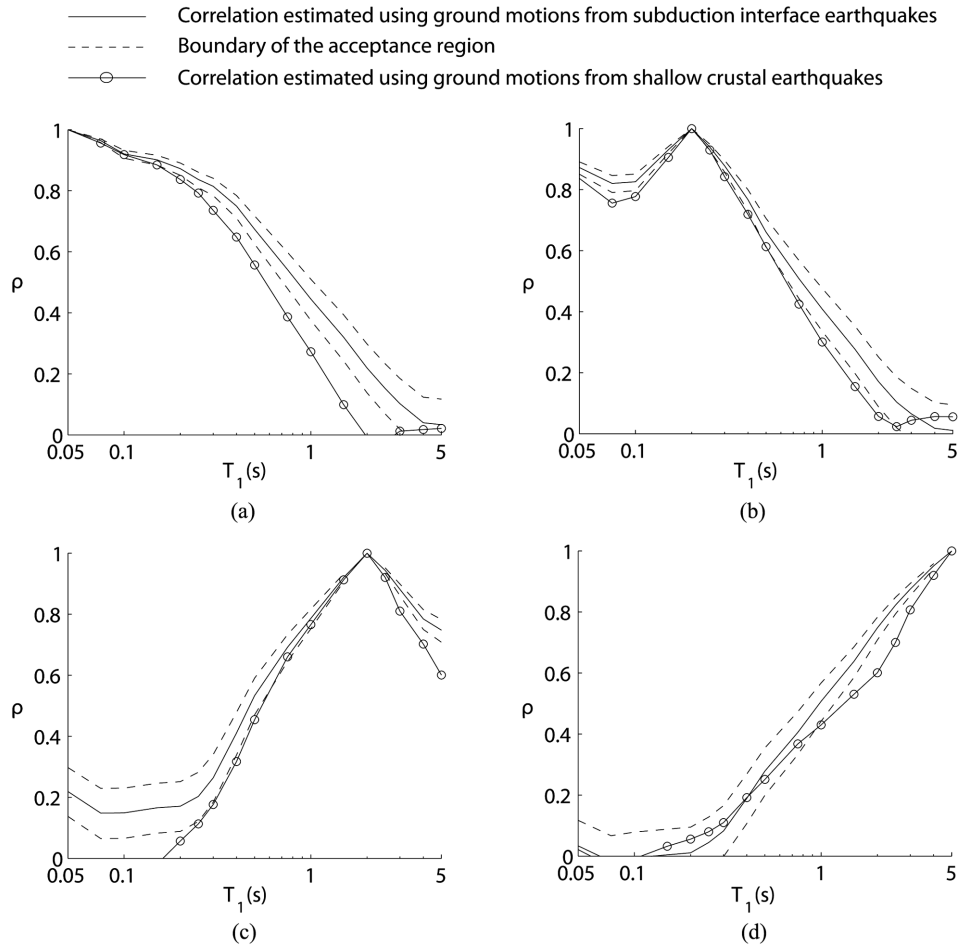
Fig. 4 Plots of correlation coefficients of $\varepsilon(T_1)$ versus $\varepsilon(T_2)$ estimated using ground motions from subduction interface zone earthquakes: (a) $T_2 = 0.05$ s, (b) $T_2 = 0.2$ s, (c) $T_2 = 2.0$ s and (d) $T_2 = 5.0$ s. Also shown are the acceptance regions and the correlation coefficients estimated using active shallow crustal earthquake ground motions

correlation estimates, but there are a limited number of ground motions from non-reverse faults, so the differences are due in part to the small sample sizes used for estimating correlations. To illustrate this, Fig. 6 shows the acceptance regions for the oblique faulting ground motion correlations for comparison to the correlations estimated using the entire ground motion data set; these acceptance regions are wider than those in Fig. 4, as there were only 124 oblique faulting ground motions, versus the 936 subduction interface zone earthquake ground motions used in Fig. 4. Also shown in Fig. 6 are corresponding correlations computed using the entire ground motion data set; in many, but not in all cases, the correlation for different oblique faulting falls within the acceptance region for the entire data set, indicating the observed differences are within the range of variation expected for data sets of this size. The differences in the normal and strike-slip faults seen in Fig. 5 are even more dramatic than those of oblique faults, however, and thus are likely not explained as being due to small sample sizes.
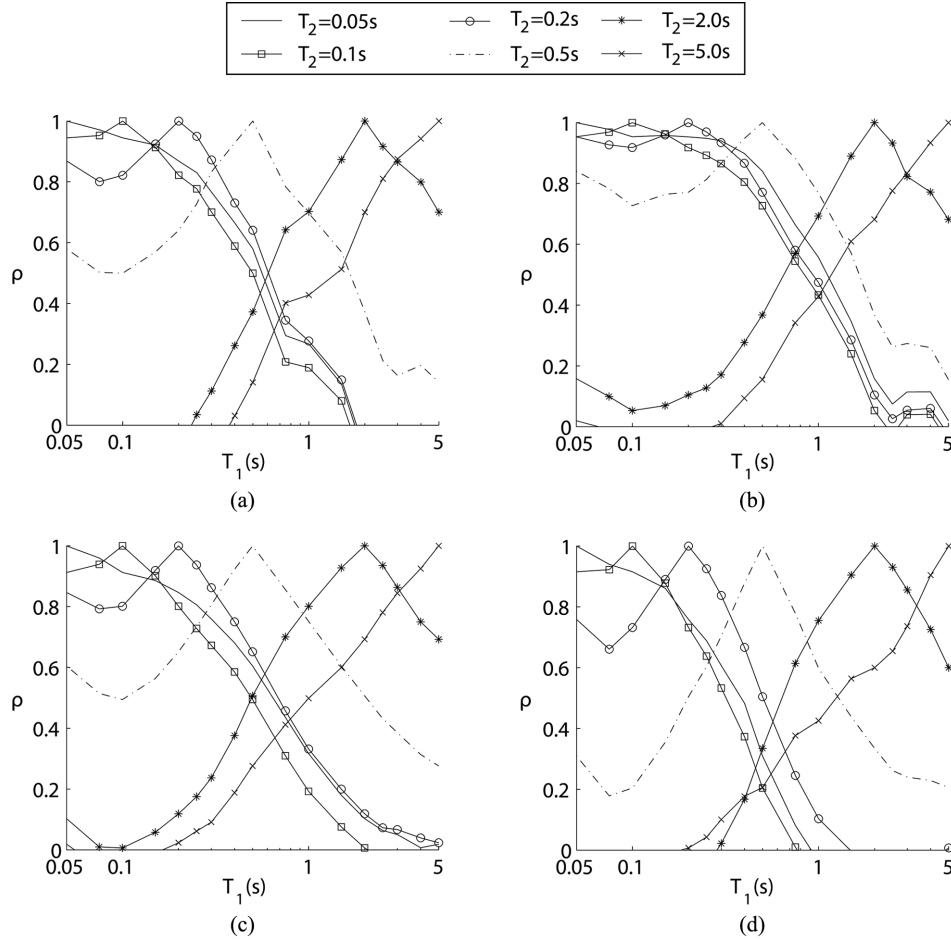
Fig. 5 Plots of correlation coefficients of $\varepsilon(T_1)$ versus $\varepsilon(T_2)$ estimated using ground motions from earthquakes on (a) normal-dip faults (232 records), (b) oblique faults (124 records), (c) reverse faults (2159 records) and (d) strike-slip faults (304 records)

Fig. 7 shows the correlation estimates obtained using ground motions recorded at rock and soil sites, where rock sites are those with $Vs30 > 760$ m/s (i.e. NEHRP site classes A and B). The rock and soil correlations are reasonably similar, with differences when T_1 or T_2 are close to 0.1s or 4s.

Fig. 8 shows acceptance regions for comparing the soil site and the rock site correlations, and shows that in approximately half of the cases the differences between rock and soil site correlations are not statistically significant. The majority of sites in the database are classified as soil sites; less than 10% of the sites are rock-sites. While these similarities may be surprising given that ground motions at soil and rock sites can differ significantly, it may be useful to note that these plots are quantifying only the residual variation in response spectra. Differences in mean response spectra are already accounted for in the $\mu_{\ln Sa}(M, R, \theta, T)$ term of Eq. (1), these differences in correlation are usually a second-order issue relative to those differences in mean values.

In order to assess the impact of source-to-site distance on the correlation, the data set is subdivided into groups of sites within 100 km of the rupture and sites farther than 100km from the
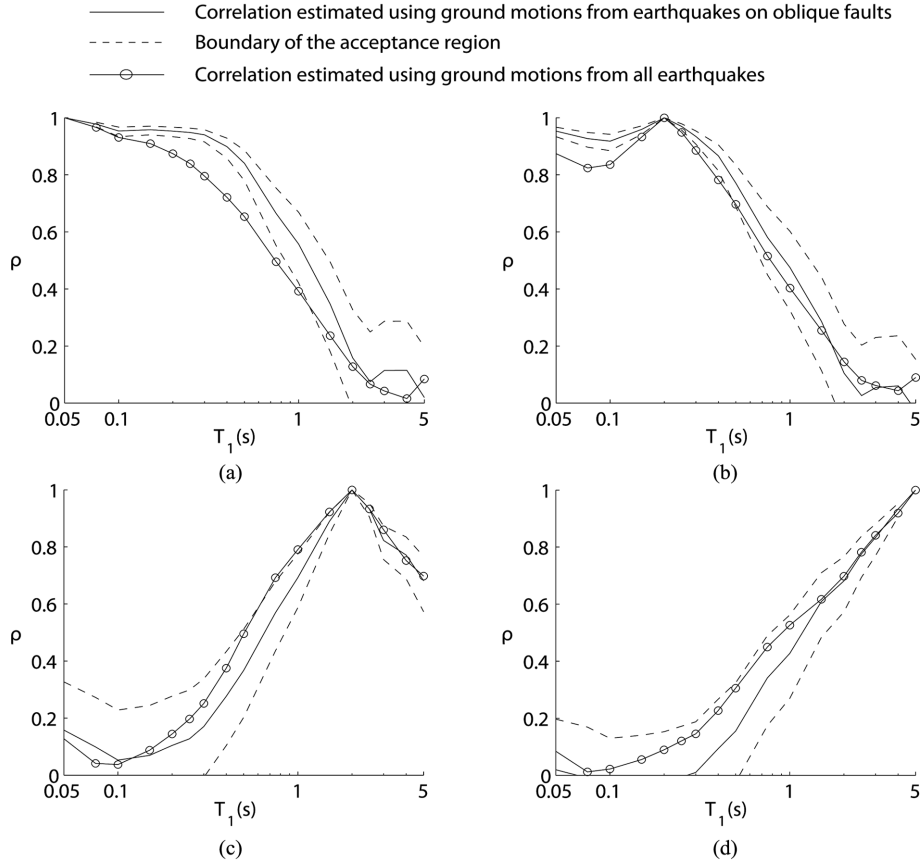
Fig. 6 Plots of correlation coefficients of $\varepsilon(T_1)$ versus $\varepsilon(T_2)$ estimated using ground motions from earthquakes on oblique faults: (a) $T_2 = 0.05$ s, (b) $T_2 = 0.2$ s, (c) $T_2 = 2.0$ s and (d) $T_2 = 5.0$ s. Also shown are the acceptance regions and the correlation coefficients estimated using all available ground motions
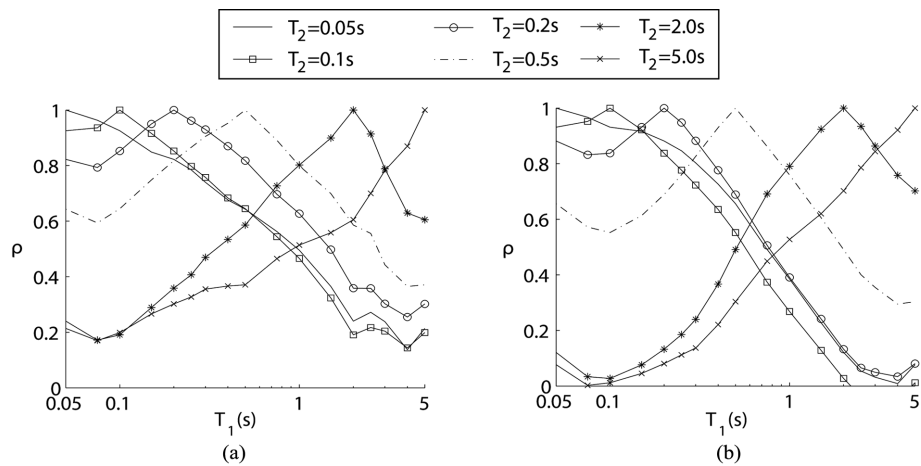
Fig. 7 Plots of correlation coefficients of $\varepsilon(T_1)$ versus $\varepsilon(T_2)$ estimated using ground motions from (a) rock sites (184 records) and (b) soil sites (2635 records)
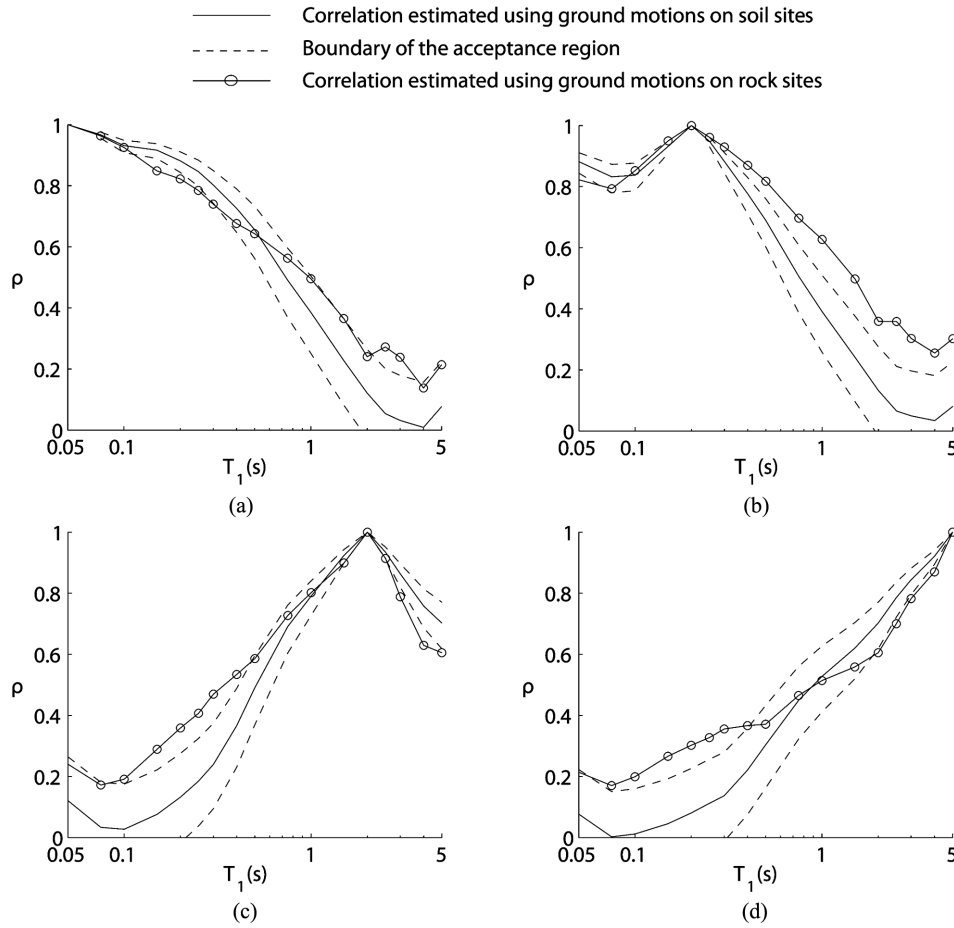
Fig. 8 Plots of correlation coefficients of $\varepsilon(T_1)$ versus $\varepsilon(T_2)$ estimated using ground motions from earthquakes on soil sites: (a) $T_2 = 0.05$ s, (b) $T_2 = 0.2$ s, (c) $T_2 = 2.0$ s and (d) $T_2 = 5.0$ s. Also shown are the acceptance regions and the correlation coefficients estimated using rock site ground motions

rupture. Fig. 9 shows the correlation estimates obtained using the data from the two distance groups. Minor differences can be seen between the correlation estimates obtained in the two cases. In general, the correlations are seen to be slightly larger at far-away sites than at nearby sites, but the differences are typically less than 0.1. This conclusion is similar to that from an earlier study, using different ground motion data but carefully studying the effect of ground motion magnitude and distance on response spectral correlations (Baker and Cornell 2005); that study also concluded that earthquake magnitude and distance did not appreciably affect response spectral correlations.

Fig. 10 shows the correlations estimated using three different ground-motion models. The Kanno *et al.* (2006) model, the Abrahamson and Silva (1997) model and the Boore and Atkinson (2008) model were all used to predict the mean values and standard deviations used in Eq. (2), and each set of resulting ε values was used to compute new sets of correlation coefficients. When using the Abrahamson and Silva (1997) and the Boore and Atkinson (2008) models, ε values were only computed for the active shallow crustal earthquake ground motions, as those models are not intended to be applicable to other seismic zones. The results obtained using the Abrahamson and
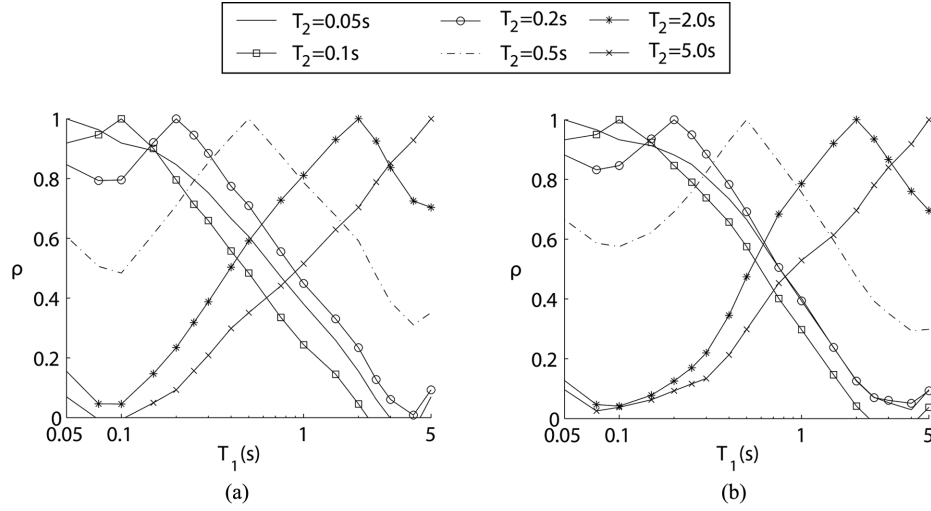
Fig. 9 Plots of correlation coefficients of $\varepsilon(T_1)$ versus $\varepsilon(T_2)$ estimated using ground motions from (a) sites within 100 km of the rupture (575 records) and (b) sites farther than 100 km of the rupture (2244 records)

Fig. 10 Plots of correlation coefficients of $\varepsilon(T_1)$ versus $\varepsilon(T_2)$ estimated using (a) the Kanno *et al.* (2006) ground motion model, (b) the Abrahamson and Silva (1997) ground motion model and (c) the Boore and Atkinson (2008) ground motion model

Fig. 11 (a) Estimated correlations coefficients of $\varepsilon(T)$ versus $\varepsilon(T)$ from orthogonal components of ground motion (North-South and East-West comp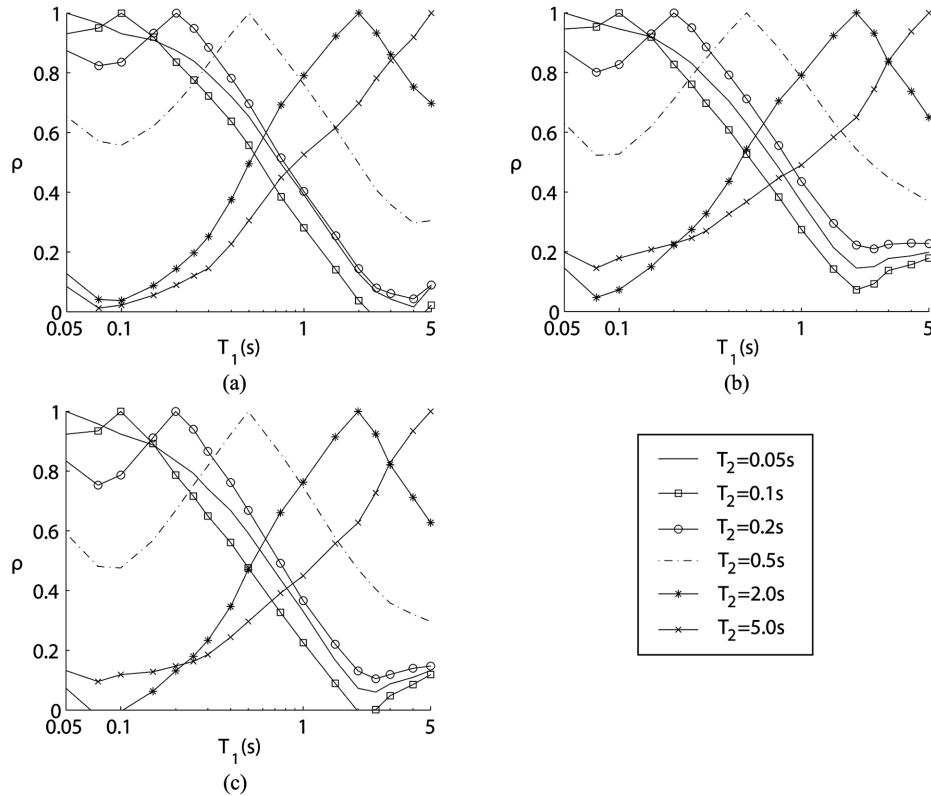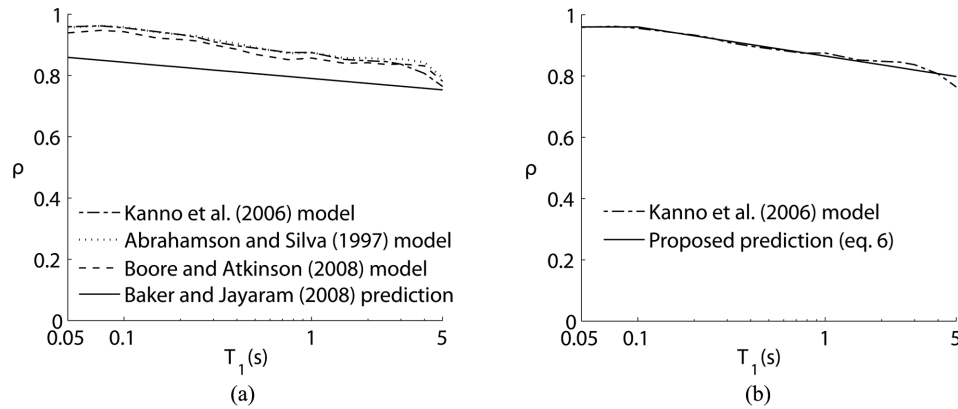onents), computed using residuals several ground motion models. (b) Estimated correlations coefficients using the Kanno *et al.* model and the regression function fit to these estimates

Silva (1997) model and the Boore and Atkinson (2008) model are similar to those observed in previous work (Baker and Jayaram 2008). Some differences are seen, however, when the Kanno *et al.* (2006) model is used when T_1 and T_2 differ significantly (in particular, when one period is shorter than 0.1s and the other longer than 2.0s). It should be noted that if the Abrahamson and Silva (1997) model or the Boore and Atkinson (2008) model are used to predict the subduction-zone Japanese earthquake data, the resulting correlations in residuals are significantly different than correlations from the Kanno *et al.* (2006) model, which is perhaps not surprising since those models are not intended for use with subduction earthquake data.

Finally, Fig. 11(a) shows empirical correlations between orthogonal-component (North-South and East-West) ground-motion spectral accelerations, where both spectral acceleration values are computed at the same period. Correlations estimated using the three ground motion models considered in Fig. 10 are shown, along with the corresponding prediction from Baker and Jayaram (2008). The correlations estimated in this study using the Japanese ground motion components are significantly higher than those predicted by the Baker and Jayaram (2008) model, which was developed using primarily U.S. ground motions. Unlike in previous figures, where any large discrepancies in correlations between predictions arose only in situations where the correlations are small, these discrepancies are occurring between highly correlated values. This is important, because discrepancies are less likely to be caused by small sample variability when correlations are high (Kutner *et al.* 2004), and because discrepancies in correlations among highly correlated variables will have greater numerical impact on calculations such as Vector Probabilistic Seismic Hazard Analysis or Conditional Mean Spectrum calculations.

Fig. 11(a) shows the correlations are not significantly affected by the choice of ground motion model, suggesting that the observation is related to the ground motions themselves rather than differences between ground motion models. Similarly, these correlations were not seen to be significantly affected by dividing the ground motions according to source mechanism, crustal zone or site classification. At present, the authors have no physical explanation for this difference relative to correlations observed in ground motion data from other regions (principally the U.S.). The following predictive equation is proposed for correlations of orthogonal ground motions at a given

period T

$$\rho_{\varepsilon_x(T), \varepsilon_y(T)} = 0.96 \qquad \text{if} \quad T < 0.1s$$
$$= 0.865 - 0.041 \ln T \quad \text{otherwise} \tag{6}$$

where $\rho_{\varepsilon_x(T), \varepsilon_y(T)}$ denotes the correlation between two epsilons, ε_x and ε_y, associated with orthogonal ground motion components at a given period T.

5. Conclusions

This paper presents the results of an effort to collect a large database of Japanese strong ground motions and study the correlation of their response spectral values at differing periods or orientations. The process used to collect and analyze the ground motions was described in detail. Spectral acceleration periods ranging from 0.05 to 5 seconds were considered when computing correlations. Observed correlation coefficients from Japanese strong motion data were compared to predictions from a model derived using ground motions from active shallow crustal earthquakes in other parts of the world (Baker and Jayaram 2008). The estimated correlations for Japanese strong motions were similar in a general sense, but not identical, to the predictive model of Baker and Jayaram.

The ground motion dataset was subdivided into separate groups, and correlations recomputed for each subgroup, to evaluate the variation in correlations between ground motions having different earthquake rupture mechanisms, alternative tectonic sources, site conditions, ground motion models, and source-to-site distances. Differences in correlations were observed and they appear to be dependent on earthquake source mechanism (faulting style) and source-to-site distance. Statistical tests were performed to evaluate the extent to which differences could be explained by systematic effects of different features, or are consistent with the observed variability associated with the present dataset. Some, but by no means all, of the variation could be explained by the effect of limited sample sizes. Most of these observed differences are correlation coefficients that vary by less than 0.2, and occur in areas where the correlation is low. Such discrepancies may not have a significant impact in many applications, but this should be determined on a case by case basis.

Correlations were also computed between spectral acceleration values from orthogonal horizontal components of a ground motion at a single period. The results suggest Japanese ground motions have higher correlations than have previously been observed in other ground motion data sets. For this reason, a new predictive equation was calibrated from the empirical data used here.

Response spectrum correlation predictions can be used as inputs to a variety of ground motion calculations such as Vector-Valued Probabilistic Seismic Hazard Analysis, Conditional Mean Spectrum calculations, and development of ground motion predictions for of spectral acceleration averaged over a period range (Baker and Jayaram 2008). There is growing interest in using these tools for assessing seismic hazard in Japan, so this study provides new information as to appropriate correlation coefficients to be used for these calculations at Japanese sites. When performing such calculations for Japanese sites, one can obtain approximate correlation predictions by using the model of Baker and Jayaram (2008). If one desires more accurate correlation coefficients computed using Japanese data (and perhaps using some specific subset of that data such as ground motions recorded on soil sites), tables of correlation coefficients have been provided.

Acknowledgements

References

Abrahamson, N.A., Kammerer, A. and Gregor, N. (2003), *Summary of scaling relations for spectral damping, peak velocity, and average spectral acceleration: report for the PEGASOS project*, Personal communication.

Abrahamson, N.A. and Silva, W. (1997), "Empirical response spectral attenuation relations for shallow crustal earthquakes", *Seismol. Res. Lett.*, **68**(1), 94-127.

Aoi, S., Obara, K., Hori, S., Kasahara, K. and Okada, Y. (2000), "New strong-motion observation network: KiK-net", *EOS Trans. Am. Geophys. Union*, **81**.

Baker, J.W. and Cornell, C.A. (2005), "Vector-valued ground motion intensity measures for probabilistic seismic demand analysis", Report No. 150, John A. Blume Earthquake Engineering Center, Stanford, CA, 321p.

Baker, J.W. and Cornell, C.A. (2006a), "Correlation of response spectral values for multi-component ground motions", *B. Seismol. Soc. Am.*, **96**(1), 215-227.

Baker, J.W. and Cornell, C.A. (2006b), "Spectral shape, epsilon and record selection", *Earthq. Eng. Struct. Dyn.*, **35**(9), 1077-1095.

Baker, J.W. and Jayaram, N. (2008), "Correlation of spectral acceleration values from NGA ground motion models", *Earthq. Spectra*, **24**(1), 299-317.

Bazzurro, P. and Cornell, C.A. (2002), "Vector-valued probabilistic seismic hazard analysis", *7th U.S. National Conference on Earthquake Engineering*, Earthquake Engineering Research Institute, Boston, MA, 10p.

Bazzurro, P., Tothong, P. and Park, J. (2009), "Efficient approach to vector-valued probabilistic seismic hazard analysis of multiple correlated ground motion parameters", *International Conference on Structural Safety and Reliability (ICOSSAR09)*, Osaka, Japan, 7p.

Boore, D.M. and Atkinson, G.M. (2008), "Ground-motion prediction equations for the average horizontal component of PGA, PGV, and 5%-damped PSA at spectral periods between 0.01 s and 10.0 s", *Earthq. Spectra*, **24**(1), 99-138.

Building Seismic Safety Council (1997), *NEHRP recommended provisions for seismic regulations for new buildings and other structures, Part 1: Provisions*, FEMA 302, Federal Emergency Management Agency.

Gulerce, Z. and Abrahamson, N.A. (2011), "Site-specific design spectra for vertical ground motion", *Earthq. Spectra*. (in press)

Inoue, T. and Cornell, C.A. (1990), "Seismic hazard analysis of multi-degree-of-freedom structures", Report #RMS-8, Reliability of Marine Structures, Stanford, CA, 70p.

Ishida, H. (1993), "Probabilistic evaluation of earthquake response spectrum and its application to response analysis", *Proceedings, 6th International Conference on Structural Safety and Reliability*, Innsbruck, Austria, 8.

Kanno, T., Narita, A., Morikawa, N., Fujiwara, H. and Fukushima, Y. (2006), "A new attenuation relation for strong ground motion in Japan based on recorded data", *B. Seismol. Soc. Am.*, **96**(3), 879-897.

Kinoshita, S. (1998), "Kyoshin Net (K-NET), *Seismol. Res. Lett.*, **69**, 309-334.

Kutner, M.H., Nachtsheim, C. and Neter, J. (2004), *Applied linear regression models*, McGraw-Hill/Irwin, Boston, New York.

Appendix: Tables of observed correlation coefficients

The following tables provide correlations computed for several sub-sets of the considered ground motions. These correlations were plotted in the figures above. These tables can be used when correlations coefficients for a specific ground motion scenario are needed.

Table 2 Correlation coefficients of $\varepsilon(T_1)$ versus $\varepsilon(T_2)$ obtained using Kanno *et al.* (2006) ground motion model. These results are plotted in Fig. 2(a)

T_2 ↓ \ T_1 →	0.05	0.08	0.10	0.15	0.20	0.30	0.40	0.50	0.75	1.00	1.50	2.00	2.50	3.00	4.00	5.00
0.05	1.00	0.97	0.93	0.91	0.87	0.80	0.72	0.65	0.50	0.39	0.24	0.13	0.07	0.04	0.02	0.08
0.08	0.97	1.00	0.95	0.89	0.82	0.73	0.65	0.57	0.40	0.30	0.15	0.04	-0.02	-0.04	-0.05	0.01
0.10	0.93	0.95	1.00	0.92	0.84	0.72	0.64	0.56	0.38	0.28	0.14	0.04	-0.02	-0.03	-0.04	0.02
0.15	0.91	0.89	0.92	1.00	0.93	0.80	0.70	0.62	0.44	0.34	0.19	0.09	0.02	0.01	0.00	0.06
0.20	0.87	0.82	0.84	0.93	1.00	0.89	0.78	0.70	0.52	0.40	0.25	0.14	0.08	0.06	0.04	0.09
0.30	0.80	0.73	0.72	0.80	0.89	1.00	0.92	0.83	0.64	0.52	0.37	0.25	0.17	0.14	0.12	0.15
0.40	0.72	0.65	0.64	0.70	0.78	0.92	1.00	0.93	0.76	0.65	0.49	0.38	0.29	0.26	0.21	0.23
0.50	0.65	0.57	0.56	0.62	0.70	0.83	0.93	1.00	0.86	0.76	0.61	0.50	0.41	0.36	0.30	0.31
0.75	0.50	0.40	0.38	0.44	0.52	0.64	0.76	0.86	1.00	0.92	0.79	0.69	0.61	0.55	0.45	0.45
1.00	0.39	0.30	0.28	0.34	0.40	0.52	0.65	0.76	0.92	1.00	0.89	0.79	0.71	0.64	0.54	0.53
1.50	0.24	0.15	0.14	0.19	0.25	0.37	0.49	0.61	0.79	0.89	1.00	0.92	0.85	0.77	0.66	0.62
2.00	0.13	0.04	0.04	0.09	0.14	0.25	0.38	0.50	0.69	0.79	0.92	1.00	0.93	0.86	0.75	0.70
2.50	0.07	-0.02	-0.02	0.02	0.08	0.17	0.29	0.41	0.61	0.71	0.85	0.93	1.00	0.95	0.85	0.78
3.00	0.04	-0.04	-0.03	0.01	0.06	0.14	0.26	0.36	0.55	0.64	0.77	0.86	0.95	1.00	0.92	0.84
4.00	0.02	-0.05	-0.04	0.00	0.04	0.12	0.21	0.30	0.45	0.54	0.66	0.75	0.85	0.92	1.00	0.92
5.00	0.08	0.01	0.02	0.06	0.09	0.15	0.23	0.31	0.45	0.53	0.62	0.70	0.78	0.84	0.92	1.00

Table 3 Correlation coefficients of $\varepsilon(T_1)$ versus $\varepsilon(T_2)$ obtained using ground motions corresponding to active shallow crustal zone earthquakes. Results are plotted in Fig. 3(a)

T_1 →																
	0.05	0.08	0.10	0.15	0.20	0.30	0.40	0.50	0.75	1.00	1.50	2.00	2.50	3.00	4.00	5.00
T_2 0.05	1.00	0.96	0.92	0.88	0.84	0.74	0.65	0.56	0.39	0.27	0.10	-0.01	-0.02	0.01	0.02	0.02
↓ 0.08	0.96	1.00	0.93	0.84	0.76	0.63	0.54	0.44	0.28	0.17	0.00	-0.11	-0.11	-0.07	-0.05	-0.03
0.10	0.92	0.93	1.00	0.89	0.78	0.62	0.52	0.42	0.26	0.15	0.01	-0.10	-0.10	-0.05	-0.03	-0.01
0.15	0.88	0.84	0.89	1.00	0.91	0.72	0.61	0.51	0.34	0.23	0.08	-0.02	-0.04	0.00	0.02	0.03
0.20	0.84	0.76	0.78	0.91	1.00	0.84	0.72	0.61	0.42	0.30	0.15	0.06	0.02	0.04	0.06	0.06
0.30	0.74	0.63	0.62	0.72	0.84	1.00	0.90	0.79	0.58	0.45	0.29	0.18	0.12	0.12	0.12	0.11
0.40	0.65	0.54	0.52	0.61	0.72	0.90	1.00	0.91	0.73	0.60	0.43	0.32	0.26	0.23	0.21	0.19
0.50	0.56	0.44	0.42	0.51	0.61	0.79	0.91	1.00	0.85	0.73	0.57	0.45	0.38	0.34	0.29	0.25
0.75	0.39	0.28	0.26	0.34	0.42	0.58	0.73	0.85	1.00	0.91	0.76	0.66	0.58	0.51	0.44	0.37
1.00	0.27	0.17	0.15	0.23	0.30	0.45	0.60	0.73	0.91	1.00	0.87	0.77	0.68	0.60	0.51	0.43
1.50	0.10	0.00	0.01	0.08	0.15	0.29	0.43	0.57	0.76	0.87	1.00	0.91	0.82	0.72	0.62	0.53
2.00	-0.01	-0.11	-0.10	-0.02	0.06	0.18	0.32	0.45	0.66	0.77	0.91	1.00	0.92	0.81	0.70	0.60
2.50	-0.02	-0.11	-0.10	-0.04	0.02	0.12	0.26	0.38	0.58	0.68	0.82	0.92	1.00	0.93	0.81	0.70
3.00	0.01	-0.07	-0.05	0.00	0.04	0.12	0.23	0.34	0.51	0.60	0.72	0.81	0.93	1.00	0.91	0.81
4.00	0.02	-0.05	-0.03	0.02	0.06	0.12	0.21	0.29	0.44	0.51	0.62	0.70	0.81	0.91	1.00	0.92
5.00	0.02	-0.03	-0.01	0.03	0.06	0.11	0.19	0.25	0.37	0.43	0.53	0.60	0.70	0.81	0.92	1.00

Table 4 Correlation coefficients of $\varepsilon(T_1)$ versus $\varepsilon(T_2)$ obtained using ground motions corresponding to subduction interface zone earthquakes. Results are plotted in Fig. 3(b)

T_1 →																
	0.05	0.08	0.10	0.15	0.20	0.30	0.40	0.50	0.75	1.00	1.50	2.00	2.50	3.00	4.00	5.00
T_2 0.05	1.00	0.96	0.92	0.90	0.87	0.81	0.75	0.67	0.54	0.45	0.32	0.22	0.15	0.10	0.04	0.03
↓ 0.08	0.96	1.00	0.94	0.87	0.82	0.74	0.67	0.59	0.46	0.36	0.25	0.15	0.09	0.04	-0.01	-0.02
0.10	0.92	0.94	1.00	0.90	0.83	0.72	0.65	0.57	0.43	0.34	0.23	0.15	0.09	0.05	0.00	-0.01
0.15	0.90	0.87	0.90	1.00	0.93	0.79	0.69	0.60	0.46	0.37	0.26	0.17	0.10	0.06	0.01	0.00
0.20	0.87	0.82	0.83	0.93	1.00	0.88	0.77	0.66	0.51	0.41	0.28	0.17	0.10	0.07	0.02	0.01
0.30	0.81	0.74	0.72	0.79	0.88	1.00	0.91	0.80	0.63	0.51	0.37	0.26	0.19	0.14	0.09	0.08
0.40	0.75	0.67	0.65	0.69	0.77	0.91	1.00	0.92	0.77	0.66	0.51	0.41	0.33	0.27	0.21	0.19
0.50	0.67	0.59	0.57	0.60	0.66	0.80	0.92	1.00	0.88	0.79	0.63	0.53	0.44	0.38	0.30	0.28
0.75	0.54	0.46	0.43	0.46	0.51	0.63	0.77	0.88	1.00	0.92	0.79	0.69	0.60	0.53	0.43	0.41
1.00	0.45	0.36	0.34	0.37	0.41	0.51	0.66	0.79	0.92	1.00	0.88	0.79	0.71	0.64	0.53	0.51
1.50	0.32	0.25	0.23	0.26	0.28	0.37	0.51	0.63	0.79	0.88	1.00	0.92	0.85	0.78	0.67	0.64
2.00	0.22	0.15	0.15	0.17	0.17	0.26	0.41	0.53	0.69	0.79	0.92	1.00	0.94	0.88	0.78	0.75
2.50	0.15	0.09	0.09	0.10	0.10	0.19	0.33	0.44	0.60	0.71	0.85	0.94	1.00	0.96	0.87	0.82
3.00	0.10	0.04	0.05	0.06	0.07	0.14	0.27	0.38	0.53	0.64	0.78	0.88	0.96	1.00	0.93	0.87
4.00	0.04	-0.01	0.00	0.01	0.02	0.09	0.21	0.30	0.43	0.53	0.67	0.78	0.87	0.93	1.00	0.95
5.00	0.03	-0.02	-0.01	0.00	0.01	0.08	0.19	0.28	0.41	0.51	0.64	0.75	0.82	0.87	0.95	1.00

Table 5 Correlation coefficients of $\varepsilon(T_1)$ versus $\varepsilon(T_2)$ obtained using ground motions corresponding to subduction slab zone earthquakes. Results are plotted in Fig. 3(c)

$T_1 \rightarrow$		0.05	0.08	0.10	0.15	0.20	0.30	0.40	0.50	0.75	1.00	1.50	2.00	2.50	3.00	4.00	5.00
T_2	0.05	1.00	0.97	0.94	0.91	0.87	0.79	0.72	0.66	0.44	0.37	0.22	0.09	-0.02	-0.04	0.01	-0.03
$\downarrow$	0.08	0.97	1.00	0.95	0.90	0.84	0.75	0.68	0.61	0.39	0.32	0.18	0.05	-0.07	-0.09	-0.03	-0.08
	0.10	0.94	0.95	1.00	0.93	0.86	0.76	0.68	0.62	0.40	0.33	0.18	0.06	-0.05	-0.06	0.01	-0.03
	0.15	0.91	0.90	0.93	1.00	0.95	0.84	0.75	0.69	0.47	0.38	0.23	0.10	0.00	-0.01	0.05	0.02
	0.20	0.87	0.84	0.86	0.95	1.00	0.91	0.82	0.76	0.54	0.45	0.30	0.16	0.07	0.05	0.10	0.07
	0.30	0.79	0.75	0.76	0.84	0.91	1.00	0.94	0.88	0.69	0.59	0.45	0.31	0.21	0.19	0.21	0.17
	0.40	0.72	0.68	0.68	0.75	0.82	0.94	1.00	0.95	0.78	0.69	0.55	0.41	0.31	0.29	0.29	0.24
	0.50	0.66	0.61	0.62	0.69	0.76	0.88	0.95	1.00	0.86	0.77	0.63	0.49	0.39	0.37	0.36	0.32
	0.75	0.44	0.39	0.40	0.47	0.54	0.69	0.78	0.86	1.00	0.93	0.82	0.70	0.62	0.58	0.50	0.47
	1.00	0.37	0.32	0.33	0.38	0.45	0.59	0.69	0.77	0.93	1.00	0.90	0.80	0.71	0.67	0.58	0.54
	1.50	0.22	0.18	0.18	0.23	0.30	0.45	0.55	0.63	0.82	0.90	1.00	0.93	0.85	0.81	0.68	0.62
	2.00	0.09	0.05	0.06	0.10	0.16	0.31	0.41	0.49	0.70	0.80	0.93	1.00	0.93	0.89	0.77	0.71
	2.50	-0.02	-0.07	-0.05	0.00	0.07	0.21	0.31	0.39	0.62	0.71	0.85	0.93	1.00	0.97	0.87	0.79
	3.00	-0.04	-0.09	-0.06	-0.01	0.05	0.19	0.29	0.37	0.58	0.67	0.81	0.89	0.97	1.00	0.91	0.84
	4.00	0.01	-0.03	0.01	0.05	0.10	0.21	0.29	0.36	0.50	0.58	0.68	0.77	0.87	0.91	1.00	0.93
	5.00	-0.03	-0.08	-0.03	0.02	0.07	0.17	0.24	0.32	0.47	0.54	0.62	0.71	0.79	0.84	0.93	1.00

Table 6 Correlation coefficients of $\varepsilon(T_1)$ versus $\varepsilon(T_2)$ obtained using ground motions from earthquakes on normal-dip faults. Results are plotted in Fig. 5(a)

$T_1 \rightarrow$		0.05	0.08	0.10	0.15	0.20	0.30	0.40	0.50	0.75	1.00	1.50	2.00	2.50	3.00	4.00	5.00
T_2	0.05	1.00	0.97	0.94	0.92	0.87	0.77	0.66	0.58	0.29	0.27	0.13	-0.10	-0.31	-0.37	-0.29	-0.32
$\downarrow$	0.08	0.97	1.00	0.95	0.88	0.80	0.69	0.59	0.50	0.23	0.22	0.11	-0.13	-0.34	-0.40	-0.32	-0.35
	0.10	0.94	0.95	1.00	0.91	0.82	0.70	0.59	0.50	0.21	0.19	0.08	-0.14	-0.34	-0.38	-0.30	-0.33
	0.15	0.92	0.88	0.91	1.00	0.92	0.79	0.65	0.57	0.27	0.23	0.11	-0.12	-0.31	-0.35	-0.26	-0.29
	0.20	0.87	0.80	0.82	0.92	1.00	0.87	0.73	0.64	0.34	0.28	0.15	-0.08	-0.24	-0.28	-0.22	-0.24
	0.30	0.77	0.69	0.70	0.79	0.87	1.00	0.91	0.83	0.56	0.47	0.33	0.11	-0.06	-0.11	-0.06	-0.10
	0.40	0.66	0.59	0.59	0.65	0.73	0.91	1.00	0.93	0.68	0.60	0.48	0.26	0.10	0.04	0.07	0.03
	0.50	0.58	0.50	0.50	0.57	0.64	0.83	0.93	1.00	0.78	0.70	0.57	0.37	0.21	0.16	0.20	0.14
	0.75	0.29	0.23	0.21	0.27	0.34	0.56	0.68	0.78	1.00	0.91	0.77	0.64	0.53	0.48	0.46	0.40
	1.00	0.27	0.22	0.19	0.23	0.28	0.47	0.60	0.70	0.91	1.00	0.84	0.70	0.56	0.51	0.50	0.43
	1.50	0.13	0.11	0.08	0.11	0.15	0.33	0.48	0.57	0.77	0.84	1.00	0.87	0.75	0.68	0.62	0.51
	2.00	-0.10	-0.13	-0.14	-0.12	-0.08	0.11	0.26	0.37	0.64	0.70	0.87	1.00	0.92	0.87	0.80	0.70
	2.50	-0.31	-0.34	-0.34	-0.31	-0.24	-0.06	0.10	0.21	0.53	0.56	0.75	0.92	1.00	0.97	0.88	0.81
	3.00	-0.37	-0.40	-0.38	-0.35	-0.28	-0.11	0.04	0.16	0.48	0.51	0.68	0.87	0.97	1.00	0.93	0.88
	4.00	-0.29	-0.32	-0.30	-0.26	-0.22	-0.06	0.07	0.20	0.46	0.50	0.62	0.80	0.88	0.93	1.00	0.94
	5.00	-0.32	-0.35	-0.33	-0.29	-0.24	-0.10	0.03	0.14	0.40	0.43	0.51	0.70	0.81	0.88	0.94	1.00

Table 7 Correlation coefficients of $\varepsilon(T_1)$ versus $\varepsilon(T_2)$ obtained using ground motions from earthquakes on oblique faults. Results are plotted in Fig. 5(b)

$T_1 \rightarrow$	0.05	0.08	0.10	0.15	0.20	0.30	0.40	0.50	0.75	1.00	1.50	2.00	2.50	3.00	4.00	5.00
T_2 0.05	1.00	0.98	0.95	0.96	0.95	0.94	0.90	0.84	0.66	0.56	0.35	0.16	0.07	0.11	0.11	0.02
↓ 0.08	0.98	1.00	0.97	0.95	0.93	0.90	0.85	0.78	0.60	0.49	0.29	0.10	0.03	0.08	0.08	-0.01
0.10	0.95	0.97	1.00	0.96	0.92	0.87	0.80	0.73	0.54	0.43	0.24	0.05	-0.03	0.04	0.04	-0.05
0.15	0.96	0.95	0.96	1.00	0.96	0.90	0.85	0.76	0.58	0.45	0.25	0.07	-0.02	0.03	0.04	-0.04
0.20	0.95	0.93	0.92	0.96	1.00	0.93	0.87	0.77	0.58	0.47	0.29	0.10	0.03	0.05	0.06	-0.03
0.30	0.94	0.90	0.87	0.90	0.93	1.00	0.95	0.87	0.68	0.56	0.37	0.17	0.07	0.09	0.11	0.01
0.40	0.90	0.85	0.80	0.85	0.87	0.95	1.00	0.95	0.78	0.66	0.48	0.28	0.17	0.17	0.18	0.09
0.50	0.84	0.78	0.73	0.76	0.77	0.87	0.95	1.00	0.88	0.77	0.57	0.37	0.26	0.27	0.26	0.16
0.75	0.66	0.60	0.54	0.58	0.58	0.68	0.78	0.88	1.00	0.91	0.74	0.57	0.48	0.50	0.45	0.34
1.00	0.56	0.49	0.43	0.45	0.47	0.56	0.66	0.77	0.91	1.00	0.84	0.69	0.63	0.60	0.53	0.43
1.50	0.35	0.29	0.24	0.25	0.29	0.37	0.48	0.57	0.74	0.84	1.00	0.89	0.84	0.77	0.71	0.61
2.00	0.16	0.10	0.05	0.07	0.10	0.17	0.28	0.37	0.57	0.69	0.89	1.00	0.93	0.82	0.77	0.68
2.50	0.07	0.03	-0.03	-0.02	0.03	0.07	0.17	0.26	0.48	0.63	0.84	0.93	1.00	0.93	0.86	0.78
3.00	0.11	0.08	0.04	0.03	0.05	0.09	0.17	0.27	0.50	0.60	0.77	0.82	0.93	1.00	0.93	0.83
4.00	0.11	0.08	0.04	0.04	0.06	0.11	0.18	0.26	0.45	0.53	0.71	0.77	0.86	0.93	1.00	0.93
5.00	0.02	-0.01	-0.05	-0.04	-0.03	0.01	0.09	0.16	0.34	0.43	0.61	0.68	0.78	0.83	0.93	1.00

Table 8 Correlation coefficients of $\varepsilon(T_1)$ versus $\varepsilon(T_2)$ obtained using ground motions from earthquakes on reverse faults. Results are plotted in Fig. 5(c)

$T_1 \rightarrow$	0.05	0.08	0.10	0.15	0.20	0.30	0.40	0.50	0.75	1.00	1.50	2.00	2.50	3.00	4.00	5.00
T_2 0.05	1.00	0.96	0.91	0.89	0.85	0.76	0.68	0.60	0.44	0.32	0.18	0.10	0.06	0.05	0.01	0.02
↓ 0.08	0.96	1.00	0.94	0.86	0.79	0.69	0.60	0.51	0.34	0.22	0.09	0.01	-0.03	-0.03	-0.06	-0.06
0.10	0.91	0.94	1.00	0.90	0.80	0.67	0.59	0.49	0.31	0.19	0.08	0.01	-0.03	-0.02	-0.04	-0.04
0.15	0.89	0.86	0.90	1.00	0.92	0.76	0.65	0.56	0.37	0.25	0.13	0.06	0.02	0.02	0.00	-0.01
0.20	0.85	0.79	0.80	0.92	1.00	0.86	0.75	0.65	0.46	0.33	0.20	0.12	0.07	0.07	0.04	0.02
0.30	0.76	0.69	0.67	0.76	0.86	1.00	0.91	0.81	0.60	0.47	0.33	0.24	0.18	0.15	0.12	0.09
0.40	0.68	0.60	0.59	0.65	0.75	0.91	1.00	0.92	0.74	0.62	0.47	0.38	0.31	0.28	0.22	0.19
0.50	0.60	0.51	0.49	0.56	0.65	0.81	0.92	1.00	0.86	0.75	0.60	0.51	0.43	0.39	0.31	0.28
0.75	0.44	0.34	0.31	0.37	0.46	0.60	0.74	0.86	1.00	0.92	0.79	0.70	0.62	0.56	0.45	0.41
1.00	0.32	0.22	0.19	0.25	0.33	0.47	0.62	0.75	0.92	1.00	0.89	0.80	0.73	0.66	0.54	0.50
1.50	0.18	0.09	0.08	0.13	0.20	0.33	0.47	0.60	0.79	0.89	1.00	0.93	0.86	0.78	0.66	0.60
2.00	0.10	0.01	0.01	0.06	0.12	0.24	0.38	0.51	0.70	0.80	0.93	1.00	0.94	0.86	0.75	0.69
2.50	0.06	-0.03	-0.03	0.02	0.07	0.18	0.31	0.43	0.62	0.73	0.86	0.94	1.00	0.95	0.84	0.78
3.00	0.05	-0.03	-0.02	0.02	0.07	0.15	0.28	0.39	0.56	0.66	0.78	0.86	0.95	1.00	0.91	0.84
4.00	0.01	-0.06	-0.04	0.00	0.04	0.12	0.22	0.31	0.45	0.54	0.66	0.75	0.84	0.91	1.00	0.93
5.00	0.02	-0.06	-0.04	-0.01	0.02	0.09	0.19	0.28	0.41	0.50	0.60	0.69	0.78	0.84	0.93	1.00

Nirmal Jayaram et al.

Table 9 Correlation coefficients of $\varepsilon(T_1)$ versus $\varepsilon(T_2)$ obtained using ground motions from earthquakes on strike-slip faults. Results are plotted in Fig. 5(d)

$T_2 \downarrow$ / $T_1 \rightarrow$	0.05	0.08	0.10	0.15	0.20	0.30	0.40	0.50	0.75	1.00	1.50	2.00	2.50	3.00	4.00	5.00
0.05	1.00	0.94	0.92	0.86	0.76	0.61	0.48	0.31	0.08	-0.04	-0.17	-0.28	-0.31	-0.27	-0.12	-0.06
0.08	0.94	1.00	0.92	0.80	0.66	0.49	0.36	0.18	-0.02	-0.12	-0.25	-0.36	-0.38	-0.35	-0.18	-0.10
0.10	0.92	0.92	1.00	0.88	0.73	0.53	0.37	0.20	0.01	-0.10	-0.22	-0.36	-0.38	-0.35	-0.19	-0.12
0.15	0.86	0.80	0.88	1.00	0.89	0.67	0.51	0.35	0.14	0.02	-0.09	-0.21	-0.25	-0.22	-0.08	-0.01
0.20	0.76	0.66	0.73	0.89	1.00	0.84	0.67	0.50	0.25	0.10	0.00	-0.12	-0.17	-0.16	-0.04	0.01
0.30	0.61	0.49	0.53	0.67	0.84	1.00	0.86	0.70	0.43	0.26	0.15	0.02	-0.02	-0.01	0.08	0.10
0.40	0.48	0.36	0.37	0.51	0.67	0.86	1.00	0.88	0.61	0.44	0.29	0.17	0.12	0.12	0.17	0.18
0.50	0.31	0.18	0.20	0.35	0.50	0.70	0.88	1.00	0.78	0.60	0.44	0.33	0.26	0.24	0.23	0.21
0.75	0.08	-0.02	0.01	0.14	0.25	0.43	0.61	0.78	1.00	0.87	0.71	0.61	0.53	0.50	0.44	0.38
1.00	-0.04	-0.12	-0.10	0.02	0.10	0.26	0.44	0.60	0.87	1.00	0.85	0.75	0.65	0.61	0.53	0.43
1.50	-0.17	-0.25	-0.22	-0.09	0.00	0.15	0.29	0.44	0.71	0.85	1.00	0.90	0.81	0.76	0.67	0.56
2.00	-0.28	-0.36	-0.36	-0.21	-0.12	0.02	0.17	0.33	0.61	0.75	0.90	1.00	0.93	0.86	0.73	0.60
2.50	-0.31	-0.38	-0.38	-0.25	-0.17	-0.02	0.12	0.26	0.53	0.65	0.81	0.93	1.00	0.95	0.79	0.65
3.00	-0.27	-0.35	-0.35	-0.22	-0.16	-0.01	0.12	0.24	0.50	0.61	0.76	0.86	0.95	1.00	0.87	0.74
4.00	-0.12	-0.18	-0.19	-0.08	-0.04	0.08	0.17	0.23	0.44	0.53	0.67	0.73	0.79	0.87	1.00	0.90
5.00	-0.06	-0.10	-0.12	-0.01	0.01	0.10	0.18	0.21	0.38	0.43	0.56	0.60	0.65	0.74	0.90	1.00